Electronic structure of Eu–C_{70} fullerides

2010 J. Phys.: Condens. Matter 22 175504

(http://iopscience.iop.org/0953-8984/22/17/175504)

J. Phys.: Condens. Matter **22** (2010) 175504 (6pp) doi:10.1088/0953-8984/22/17/175504

Electronic structure of Eu–C_{70} fullerides

Peng Wang[1], Liang Meng[1], Xiao-Bo Wang[1], Yan-Jun Li[1], Chun-Qi Sheng[1], Wen-Hua Zhang[2], Yang Xu[2], Fa-Qiang Xu[2], Jun-Fa Zhu[2] and Hong-Nian Li[1,3]

[1] Department of Physics, Zhejiang University, Hangzhou 310027, People's Republic of China
[2] National Synchrotron Radiation Laboratory, University of Science and Technology of China, Hefei 230029, People's Republic of China

E-mail: Phylihn@public.zju.edu.cn (Hong-Nian Li)

Received 9 January 2010, in final form 11 March 2010
Published 12 April 2010
Online at stacks.iop.org/JPhysCM/22/175504

Abstract
The electronic structure of Eu-intercalated C_{70} has been studied by a synchrotron radiation photoemission spectroscopy technique. At low intercalation levels (below the stoichiometry of Eu_3C_{70}), the photoemission data clearly exhibit charge transfer from Eu 6s states to the lowest-unoccupied-molecular-orbital (LUMO) and the LUMO + 1 of C_{70}. The amount of charge transfer reaches its maximum far before intercalation saturation. Detailed analysis reveals that most of the 5d6s electrons of Eu occupy the so-called interstitial states in the saturation phase (Eu_9C_{70}). The interstitial states are induced by a Eu sub-lattice formed at heavy intercalation levels, and comprise substantial 6s-π hybridized states. The π states participating in the hybridization are mainly the HOMO $- n$ ($n = 6$–10) orbitals. The PES data also reveal the semiconducting property for both Eu_3C_{70} and Eu_9C_{70}. The 6s–(HOMO $- n$) hybridization and the semiconducting property should play important roles in understanding the ferromagnetic mechanism for Eu_9C_{70}.

1. Introduction

C_{60} fullerides have exhibited many novel properties, such as superconductivity [1–6], ferromagnetism [7–9] and giant magnetoresistance [7]. Superconductivity has not been observed in higher (C_{70}, C_{84}, etc) fullerides to date, probably due to the lower symmetries of the higher fullerene molecules and the related lattice disorder of the fullerides. However, the finding of ferromagnetic Eu_9C_{70} [10] implies that a fullerene-based magnet is not prohibited by the lower symmetries. To understand the mechanism of the magnetism for fullerene-based materials, knowledge about the electronic structure is needed. Photoemission spectroscopy (PES) is one of the most powerful tools to investigate the electronic structure. However, to the best of our knowledge, there is no PES data of rare-earth metal-intercalated C_{70} in the literature.

In this paper, we report our PES study of Eu–C_{70} fullerides. We prepared Eu-intercalated C_{70} films in an ultra-high vacuum and measured the PES data. *Ab initio* molecular orbital calculations of C_{70} were performed to help to understand the spectra. The results reveal the semiconducting property for Eu_3C_{70} and Eu_9C_{70} and a limitation in the charge transfer from Eu to C_{70}. Most 5d6s electrons in Eu_9C_{70} occupy the interstitial states, which are induced by the Eu sub-lattice formed at high intercalation levels and comprise substantial 6s-π hybridized states. The π states of C_{70} involved in the hybridization are mainly the HOMO $- n$ ($n = 6$–10) orbitals, indicating the important role of the deeper molecular orbitals in determining the structural and electronic properties of fullerides.

[3] Author to whom any correspondence should be addressed.

2. Experimental details

Sample preparation and measurements were performed at the Surface Science Station of the National Synchrotron Radiation Laboratory of China (NSRL), where Al Kα source was used as a supplementary light source. The base pressure was 8×10^{-11} mbar. An angle-resolved electron energy analyzer was used to record the photoelectrons. The total energy resolution in the synchrotron radiation photoemission spectroscopy (SRPES) measurements was ~0.1 eV with the incident photon energies around 21.0 eV and got slightly worse with higher photon energies. All SRPES were measured at normal emission. X-ray photoemission (XPS, Al Kα source) data were measured after the SRPES measurements for some intercalation levels, which could estimate sample stoichiometries, monitor oxidation and study the valence state of Eu ions.

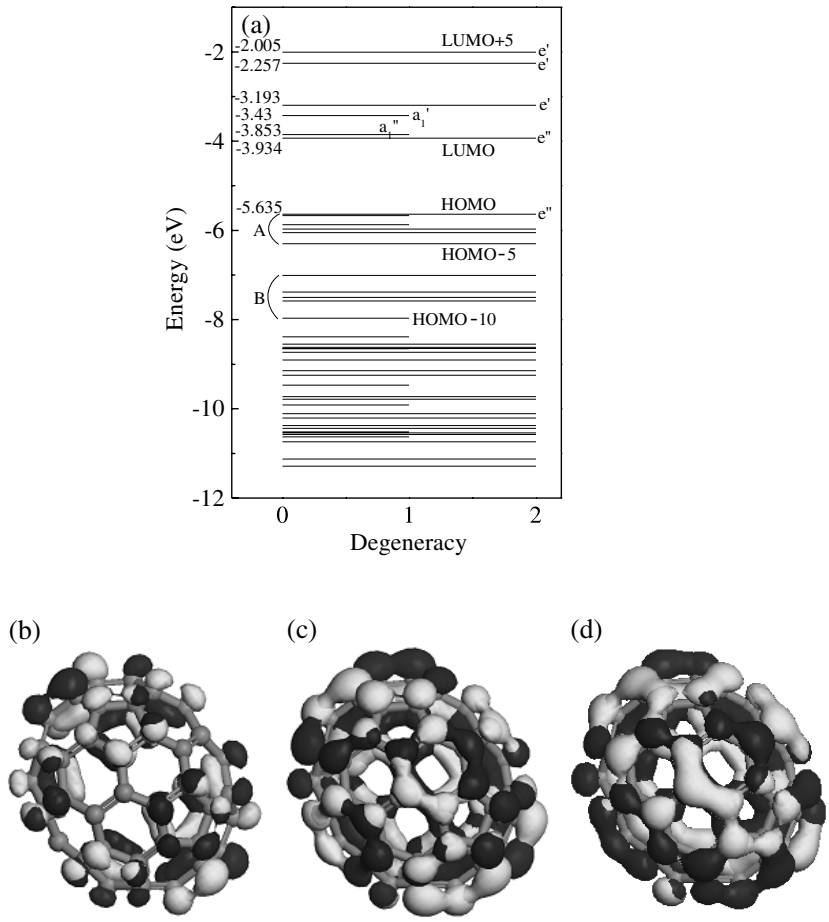

Figure 1. (a) Energy-level diagram of the C_{70} molecule. The energy values and symmetries are labeled for some levels. The labels 'A' and 'B' indicate the special bundles of energy levels corresponding to the PES features A and B in figure 2. (b)–(d) Superimposed orbitals of LUMO and LUMO + 1 (b), from HOMO to HOMO-5 (c), and from HOMO-6 to HOMO-10 (d).

C_{70} and Eu were sublimed from Knudsen cell evaporators (THC-40-10-SH, CREATEC Co., Germany) onto Si:H(111) substrates. The substrates were transferred into a vacuum chamber immediately after HF acid etching, and degassed at 300 °C for 1 h. The C_{70} source was single crystals that had been ground into a powder using an agate mortar before filling into the evaporator. The high-purity Eu (99.99%) was purchased from Beijing Research Institute for Nonferrous Metals.

A C_{70} film with thickness of ∼200 Å was prepared on the Si:H(111) substrate. The thickness of the film was estimated based on Si 2p signal attenuation and the inelastic-mean-free-path (IMFP) data, with the assumption of the IMFP of C_{70} being nearly the same as that of C_{60} [11]. The intercalation of Eu was carried out step-by-step. For each trial, we evaporated a certain amount of Eu atoms onto the surface of the C_{70} film with the substrate kept at suitable temperatures (between 150 and 240 °C). To assure homogeneous stoichiometries, the samples were subjected to a further annealing at 190 °C for 15 min for most of the trials. Once the sample had cooled down to room temperature, it was transferred from the preparation chamber into the analyzer chamber for valence band SRPES measurements ($h\upsilon = 30.5$ eV). The intercalation was continued until the XPS signal of C_{70} was almost completely attenuated. Then we deposited a large quantity of Eu atoms onto the sample surface to form a metal Eu film to determine the Fermi level.

Another sample with the stoichiometry of $Eu_{\sim 3}C_{70}$ was prepared for photon-energy-dependent PES measurements ($h\upsilon = 21.5$, 33.0, 98.0, and 141.0 eV). The spectra allowed us to read the binding energy (BE) of the 4f level at photon energies that have large photoionization cross-sections for the 4f electrons, and could be used to verify some conclusions drawn from the first sample.

Ab initio calculations of the energy-level diagram and the spatial distributions of the molecular orbitals of C_{70} were performed with the DMol^3 package [12, 13] based on density functional theory (DFT). The calculation details can be found in [14].

3. Results and discussion

Figure 1 shows the results of the DFT calculations, which will be frequently referred to throughout the discussion of the experimental data. Panels (b)–(d) illustrate the superimpositions of some special molecular orbitals, for example, panel (d) is the superimposition of nine orbitals from HOMO-6 to HOMO-10 (note that the two-fold degenerated levels have two orbitals). We construct the superimpositions

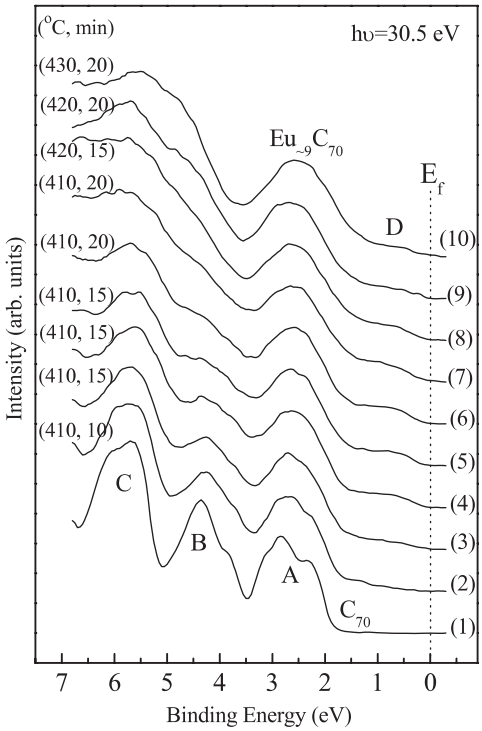

Figure 2. SRPES of Eu-intercalated C_{70} films. The temperatures of the Eu evaporation source and the deposition time are shown beside the lines for each deposition trial. The bottom line is the spectrum of pristine C_{70}. The spectral lines are normalized to the height of feature A.

because they correspond to special spectral features (see below).

The SRPES data of Eu-intercalated C_{70} films (the first sample) are shown in figure 2. The amount of Eu deposited on the sample (proportional to the temperature of the evaporation source and the deposition time) for each intercalation trial is indicated beside the spectral lines. The temperatures of the substrate during Eu deposition are 150 °C for lines (2)–(6), 170 °C for line (7), 190 °C for line (8), and 240 °C for lines (9) and (10). The annealing temperature is 190 °C for all intercalation trials except line (9). We did not anneal the sample of line (9) because we found in the experimental procedure that the intensity ratio between feature D and A decreased from line (7) to (8), and suspected that annealing at 190 °C desorbed some Eu from the sample. The result of line (9) precluded our suspicion, and annealing was resumed in line (10).

Sample stoichiometries and the valence state of Eu ions need to be specified before the discussion of figure 2. The stoichiometries are estimated by the XPS data shown in figure 3(a). The signal-to-noise ratio and the resolution are unsatisfactory because the photon flux of the x-ray source is too small and the spectra were recorded with a large pass energy (100 eV). However, we can still quantitatively estimate the sample stoichiometry for line (10) by the Eu $4p_{3/2}$/(C 1s + Eu $4p_{1/2}$) intensity ratio (the adjacent C 1s and Eu $4p_{1/2}$ peaks cannot be resolved by the low-resolution XPS measurement). This ratio is determined to be 0.42 (the Shirley backgrounds of the spectral peaks were subtracted before calculating the peak areas), which is near the anticipated value of 0.40 for Eu_9C_{70} based on the photoionization cross-section data [15]. Therefore figure 2 covers the SRPES data from pure C_{70} (line (1)) to $Eu_{\sim 9}C_{70}$ (line (10)). Figure 3(a) also reveals that the decreased intensity ratio between feature D and A from line (6) to (10) in figure 2 is not due to the decreased Eu concentration, since the XPS signal of Eu is substantially enhanced in line (10) as compared with line (7). As mentioned in section 2, our experimental procedure proceeded with several additional intercalation trials after the measurements of spectrum (10). The XPS data exhibited drastically increased signals from the core levels of Eu, verifying the intercalation saturation at line (10), and thus the data of the additional trials are not presented here. The sample stoichiometries for intermediate intercalation levels are difficult to estimate because the Eu $4p_{3/2}$ photoemission is too weak in lines (1), (4) and (7). However, by inspection of the relative intensities between Eu 4d and C 1s signals, we can at least say that lines (4) and (7) correspond to the stoichiometries less than and greater than Eu_3C_{70}, respectively. Eu–C_{70} fullerides have two stable phases of Eu_3C_{70} and Eu_9C_{70} and an intermediate phase (the stoichiometry and the crystal structure of which are unknown) between them. The intermediate phase is less stable and should have a small component in the samples [10]. So lines (1)–(4) correspond to the mixture of pristine C_{70} and Eu_3C_{70}, while lines (7)–(9) are the mixture of Eu_3C_{70}, Eu_9C_{70} and a minor amount of the intermediate phase.

Line (7) in figure 3(b) exhibits divalent Eu 3d photoemission ($4f^7$ configuration). Please note that the peak labeled with * originates either from the accompanying peak of divalent Eu $3d_{5/2}$ [16, 17], or the peak of trivalent Eu $3d_{5/2}$. By comparing the relative intensity between peak * and the main peak with that of metal Eu reported in [16], we can determine that the valence state of Eu is divalent in line (7). Considering the fact that line (7) corresponds to the mixture of different phases, we conclude that the valence state of Eu is divalent for all the phases of Eu–C_{70} fullerides, coinciding with the conclusion drawn from the x-ray absorption near edge structure (XANES) measurements [10]. The obviously enhanced peak * of line (10) in figure 3(b) should be caused by sample oxidation that resulted in trivalent Eu. Line (10) in figure 3(a) indeed exhibits obvious an O 1s signal. Eu is very sensitive to oxygen. The number of Eu ions on the top of the sample increased at higher stoichiometries. It might be inevitable that part of these top-layer Eu ions got oxidized due to the lengthy experimental procedure even though the vacuum condition was fairly well maintained. However, the oxygen contamination is negligible below the intercalation level of line (7).

Keeping in mind the sample stoichiometries and the divalent state of Eu, we now discuss the spectra in figure 2. The bottom line is the spectrum of pristine C_{70} with three features (labeled with A, B and C) between the Fermi level and 7 eV BE. These features correspond to the special bunches of energy levels of C_{70} by comparing line (1) with figure 1(a). For example, feature A corresponds to the energy levels from HOMO to HOMO-5. The schematic illustrations of the molecular orbitals (figures 1(c) and (d)) reveal that features A and B are π states (feature C does not feature much in

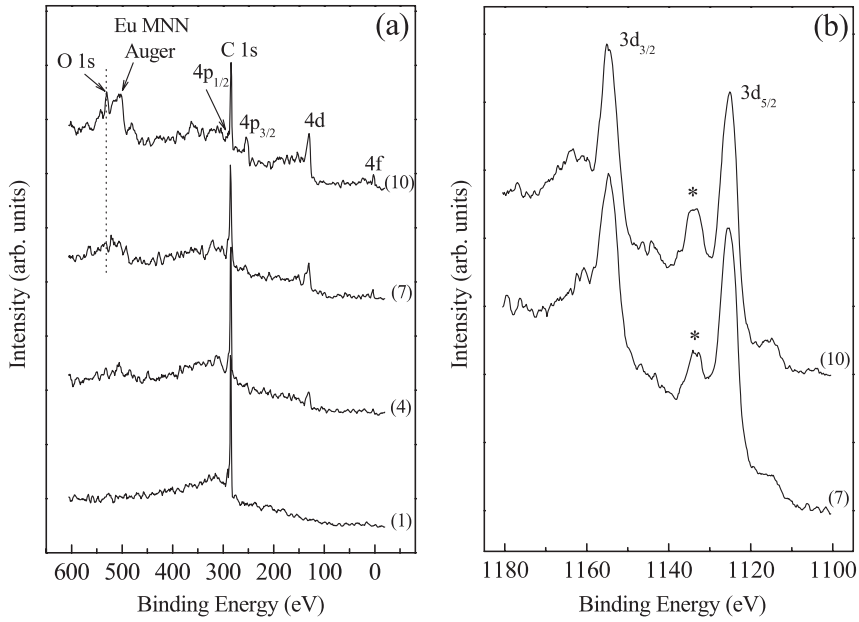

Figure 3. (a) XPS survey scanning with the pass energy of 100 eV at various intercalation levels. The parenthesized numbers next to the lines indicate that the XPS data were recorded at the intercalation levels with the same labels as in figure 2. (b) Eu 3d core-level spectra measured with the pass energy of 50 eV at two intercalation levels. The spectra are normalized to the height of the main peak of the $3d_{5/2}$ photoemission to highlight the change of the peak labeled with '$*$'. All the XPS data were measured at an emission angle of 45° with respect to sample normal.

the following discussion of the PES data, and we did not analyze its orbitals). Unlike most of the reported PES data in the literature, feature B in figure 2 has sufficient spectral intensity because we adopted the appropriate photon energy of 30.5 eV [18]. Feature D in lines (2)–(10) is induced by the electron doping from Eu.

There are some noticeable observations in the spectral evolution upon Eu intercalation, which can give much information about the electronic structure of Eu–C_{70} fullerides. First, there is no Fermi edge at any intercalation level. This observation reveals that all the phases of Eu–C_{70} fullerides are semiconducting. Although the spectrum of Eu_9C_{70} (line (10)) is greatly affected by the sample oxidation, we can draw the conclusion of Eu_9C_{70} being semiconducting based on lines (7) and (8) (O contamination is negligible for the sample of line (7), and should be mild for the sample of line (8)). The samples corresponding to lines (7) and (8) contain some Eu_9C_{70} component. If Eu_9C_{70} were metallic, we should have observed the Fermi edge.

Second, the intensity ratio between feature D and A increases from line (2) to (5), is nearly invariant from line (5) to (7), and then decreases from line (7) to (10). The increasing D/A ratio from line (2) to (5) can be easily understood as more electrons being transferred from Eu to the unoccupied molecular orbitals of C_{70} with greater Eu intercalation. There may be two reasons for the variation of the D/A ratio from line (5) to (10). One of the reasons is the Eu 4f photoemission of the increased number of Eu ions in the sample. The photoionization cross-section of Eu 4f is not negligible when compared with that of C 2p at photon energies around 30.5 eV [15, 19], and figure 4 exhibits that the 4f signal is superimposed on feature A. The other reason is that there exists a limitation in the charge transfer (see below).

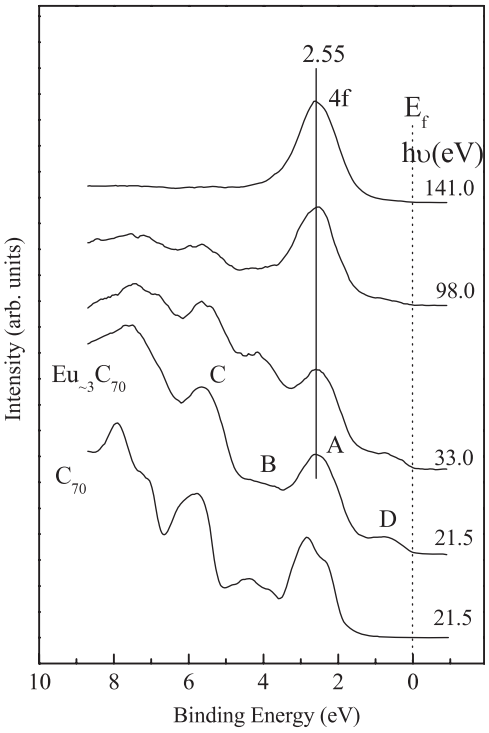

Figure 4. Photon-energy-dependent SRPES of $Eu_{\sim 3}C_{70}$. The spectral lines are normalized to the height of feature A. The bottom line is the spectrum of pristine C_{70}.

The third observation in the spectral evolution is that the peak position of feature A and the width of feature D are nearly invariant for all intercalation levels (from line (2) to (10)). The two-fold degenerate LUMO (e'') and the non-degenerate LUMO + 1 (a_1'') of C_{70} are very close in energy

(these two orbitals are π states, see figure 1(b)), and can accommodate up to six electrons. As each divalent Eu ion has two 5d6s electrons, the LUMO and LUMO + 1 orbitals should be fulfilled at the intercalation level of Eu_3C_{70} (around line (5) or (6) in figure 2) if we suppose that all the 5d6s electrons transfer to C_{70}. The next unoccupied molecular orbital, the LUMO + 2 (a_1'), is higher in energy than the LUMO + 1 by more than 0.4 eV. If this orbital is filled, feature A and other occupied bands would move towards higher binding energy due to the Fermi level shift, as in the cases of Yb and Sm intercalated C_{60} [20–22]. However, the movements are not observed in figure 2. So there exists a limitation in the charge transfer. The existence of the limitation in Eu–C_{70} fulleride can be understood by inspection of the energy-level diagram (figure 1(a)). If all the 5d6s electrons transfer to C_{70} in Eu_9C_{70}, the LUMO + 5 would be occupied. The energy of the LUMO + 5 is too high, and thus the charge transfer is destined to be incomplete. The PES data of the present work further reveal that the limitation is the filling of the LUMO + 1 derived band, and that the sample stoichiometry corresponding to the limitation is near Eu_3C_{70} (if, to say the least, not exactly Eu_3C_{70}).

A question then arises. Where are the remaining 5d6s electrons in Eu_9C_{70}? We noted that the limitation in the charge transfer was already encountered in Eu–C_{60} fullerides [23, 24] and heavily intercalated Na superfullerides [25]. For Eu–C_{60} fullerides (also exhibiting the semiconducting property for all phases and the divalent state of Eu ions), the 5d6s electrons transferred steadily to C_{60} until intercalation saturation (the ferromagnetic phase of Eu_6C_{60}) [24], but the amount of the charge transfer was no more than one electron per Eu ion. Yoshikawa *et al* [23] and Wang *et al* [24] suggested 5d6s-π hybridization as being responsible for the incomplete charger transfer (this interpretation may not be perfect, see below). For Na superfullerides, Andreoni *et al* [25] interpreted the limitation in the charge transfer as the so-called interstitial states that trapped a part of the excess electrons. The interstitial states related to the non-rigid band behavior induced by the specific structure of the Na superfullerides. In the present work, we may as well refer to the states accommodating the remaining 5d6s electrons in Eu_9C_{70} as the interstitial states. Of course, the detail and the origin of the interstitial states in Eu_9C_{70} should have substantial differences from that in Na superfullerides, as discussed in the following.

The 6s states of atomic Eu are the highest occupied level, and the 5d states are empty. For metal Eu, the maximal density of states of the 6s states (BE = 5.15 eV) falls below the 4f level (BE = 2.1 eV) by 3.05 eV, and the 5d states are partially occupied [19, 26, 27]. In the combination of Eu with C_{70}, the 6s electrons can surely transfer to the unoccupied molecular orbitals of C_{70} at lower intercalation levels (below Eu_3C_{70}) due to the electronegativity difference between the Eu atom and C_{70} molecule (the Eu–Eu distance in Eu_3C_{70} exceeds 5.61 Å [10], so the concept of electronegativity applies). We can thus observe the increasing intensity of feature D from line (2) to (5) in figure 2, and say that the bonding nature of Eu_3C_{70} is mainly ionic (with possibly some amount of covalent contribution as the case of $Yb_{2.75}C_{60}$ [28]). At higher intercalation levels, Eu_9C_{70} forms. In Eu_9C_{70}, the octahedral interstitial sites (O-sites) of the fcc lattice are multiply occupied [10]. These multiply intercalating Eu ions distribute in the center of the O-site and the vertexes of a cuboctahedron around the center, forming a Eu cluster with the Eu–Eu distance of 4.085 Å very near that of metal Eu (3.967 Å). Those Eu ions at the tetrahedral interstitial sites (T-sites) connect the neighboring cuboctahedrons (the nearest distance between the T-site Eu ion and the Eu ion at the vertex of the cuboctahedron is 3.964 Å, smaller than the Eu–Eu distance in metal Eu). Therefore the Eu ions in Eu_9C_{70} constitute a three-dimensional sub-lattice with the Eu–Eu distances near that of metal Eu (the coordination of the Eu ions in the sub-lattice, however, is less than metal Eu because not all the interstitial sites are occupied [10]). The electronic structure of the sub-lattice should mimic that of metal Eu, rather than the Eu atom. That is to say, the 6s states become lower in energy, and some 5d states fall below the Fermi level. Accordingly, charge transfer to the LUMO+2 and higher molecular orbital derived bands cannot occur, and even possibly, some electrons of the LUMO and LUMO + 1 derived bands now reversely fill the 5d states.

The lowered (in energy) 5d6s states are thus one of the origins of the interstitial states. The π states of C_{70} should be another origin. The nearest Eu–C distances between the T-site, the vertex of the cuboctahedron and the C_{70} molecule in Eu_9C_{70} are shorter than the sum of the ionic radius of Eu and the van der Waals radius of C [10], which certainly results in the 5d6s-π hybridization. Therefore the nature of the interstitial states should be 5d6s together with the hybridized states. By the way, we think that the interstitial states can be applied to understanding the electronic structure of Eu_6C_{60} as well. The hybridized states in Eu_6C_{60} have been suggested by some authors [7, 23, 24], as mentioned above, but the lowered 5d6s states were not paid sufficient attention. Actually, the Eu ions in Eu_6C_{60} also constitute a three-dimensional sub-lattice with the Eu–Eu distances near that of metal Eu [7, 8].

The last (and the fourth) meaningful observation of the spectral evolution in figure 2 is that the shape of feature B varies remarkably at high intercalation levels, which affords more information about the 5d6s-π hybridization. Feature B loses its peak and is combined into feature C as a shoulder when the stoichiometry is beyond Eu_3C_{70} (from line (6) to (10)). Although lines (9) and (10) are affected by the O 2p photoemission that generally distributes between 4.5 and 6.5 eV BE, lines (6) and (7), which were recorded when the O contamination is negligible, have already undoubtedly exhibited the drastic variation of feature B. These observations reveal the strong hybridization of feature B with the 6s states, which coincides with the special electronic structures of the Eu sub-lattice and C_{70} molecule. As mentioned above, the 6s states become lower in energy and some 5d states fall below the Fermi level. We can reasonably suppose that the maximal density of states of the 6s states is below the 4f level by ∼2 eV (somewhat less than the BE difference of 3.05 eV [19] in metal Eu by considering the fact that the atomic density of the sub-lattice is smaller than that of metal Eu). Since the energy position of the 4f level is nearly the same as feature A (see figure 4), the 6s states can match feature B in

energy distribution. The 6s states are the outermost atomic-shell, and feature B is the most extended state of C_{70} (see figure 1(d)). Therefore, the 6s states can certainly hybridize with feature B, resulting in the remarkable variation of the peak shapes. Feature B corresponds to the deeper molecular orbitals (HOMO $-$ n, n = 6–10, see figure 1(a)) of C_{70}. Although the deeper molecular orbitals are of little significance for most C_{60} fullerides, this work for the first time reveals their importance in heavily intercalated higher fullerides. Of course, we do not preclude the possibility that the π states involved in the hybridization include the molecular orbitals in a large energy range from the LUMO + 1 to the HOMO-10. However, the hybridization of the molecular orbitals from the LUMO + 1 to the HOMO-5 (corresponding to features D and A) should be less significant because only a minor amount of the 6s states are energetically compatible with these orbitals.

Figure 4 shows the photon-energy-dependent spectra of the second sample. This sample has a stoichiometry around Eu_3C_{70} (the Eu 4d/C 1s intensity ratio of this sample is intermediate between that of line (4) and (7) in figure 3(a)), and is free of oxygen contamination. At photon energies of 21.5 and 33.0 eV, the 4f signal cannot be resolved from the photoemission of the valence band of C_{70}. The Eu 4f signal prevails over the C 2p signals at a photon energy of 98.0 eV, and dominates the spectrum at the 4d–4f resonant energy (141.0 eV). Then we can read the binding energy of 2.55 eV for the 4f level in Eu_3C_{70}, which is nearly the same as feature A. The binding energy of the 4f level in Eu_9C_{70}, though not measured, should not differ substantially from that in Eu_3C_{70}, because of the inner-shell nature of the 4f level. Figure 4 also verifies that the valence state of Eu is divalent, because there is no photoemission at ∼7 eV in the top line (Eu^{3+}, if it exists, is located at ∼7 eV [29, 30]).

4. Conclusions

We have studied the electronic structure of Eu–C_{70} fullerides. Both Eu_3C_{70} and Eu_9C_{70} are semiconducting. The topmost filled state of C_{70} is the LUMO + 1 derived band, and the amount of charge transfer from Eu to C_{70} is no more than 6e per molecule. The excess 5d6s electrons in Eu_9C_{70} distribute in the interstitial states, which are constituted with the 5d6s states of the Eu sub-lattice and some 5d6s-π hybridized states. The electronic states involved in the hybridization are mainly the 6s states of Eu and the (HOMO $-$ n) (n = 6–10) orbitals of C_{70}. Our work can shed some light on the ferromagnetic mechanism for Eu_9C_{70}. Eu_9C_{70} is a ferromagnetic semiconductor, and the 6s–(HOMO $-$ n) hybridization should play an important role in the ferromagnetic coupling. The present work also reveals that the deeper molecular levels of fullerenes, say, from the HOMO-6 to the HOMO-10 for C_{70}, can be crucial to some physical properties such as magnetism, in comparison with the LUMO and LUMO + 1 levels that determine the transport properties.

Acknowledgments

This work is supported by the National Natural Science Foundation of China under Grant No. 10674115 and the National Synchrotron Radiation Laboratory of China.

References

[1] Hebard A F, Rosseinsky M J, Haddon R C, Murphy D W, Glarum S H, Palstra T T M, Ramirez A P and Kortan A R 1991 *Nature* **350** 600
[2] Rosseinsky M J, Ramirez A P, Glarum S H, Murphy D W, Haddon R C, Hebard A F, Palstra T T M, Kortan A R, Zahurak S M and Makhija A V 1991 *Phys. Rev. Lett.* **66** 2830
[3] Baenitz M, Heinze M, Lüders K, Werner H, Schlögl R, Weiden M, Spam G and Steglich F 1995 *Solid State Commun.* **96** 539
[4] Gogia B, Kordatos K, Suematsu H, Tanigaki K and Prassides K 1998 *Phys. Rev.* B **58** 1077
[5] Özdas E, Kortan A R, Kopylov N, Ramirez A P, Siegrist T, Rabe K M, Bair H E, Schuppler S and Citrin P H 1995 *Nature* **375** 126
[6] Akada M, Hirai T, Takeuchi J, Yamamoto T, Kumashiro R and Tanigaki K 2006 *Phys. Rev.* B **73** 094509
[7] Ishii K, Fujiwara A, Suematsu H and Kubozono Y 2002 *Phys. Rev.* B **65** 134431
[8] Margiolaki I, Margadonna S, Prassides K, Hansen T, Ishii K and Suematsu H 2002 *J. Am. Chem. Soc.* **124** 11288
[9] Ksari-Habiles Y, Claves D, Chouteau G, Touzain P, Jeandey Cl, Oddou J L and Stepanov A 1997 *J. Phys. Chem. Solids* **58** 1771
[10] Takenobu T, Chi D H, Margadonna S, Prassides K, Kubozono Y, Fitch A N, Kato K and Iwasa Y 2003 *J. Am. Chem. Soc.* **125** 1897
[11] Li H N, Wang X X and Ding W F 2006 *J. Electron Spectrosc. Relat. Phenom.* **153** 96
[12] Delley B 1990 *J. Chem. Phys.* **92** 508
[13] Delley B 2000 *J. Chem. Phys.* **113** 7756
[14] Li H N, Yang H, Wang X X, Ni J F, Wang P, Meng L, Wang X B, Kurash I, Qian H J, Wang J O and Liu Z Y 2009 *J. Phys.: Condens. Matter* **21** 265502
[15] Yeh J J and Lindau I 1985 *Atomic Subshell Photoionization Cross Section and Asymmetry Parameters: 1 ⩽ Z ⩽ 103* (New York: Academic) pp 7–11
[16] Wang X X, Li H N and Xu Y B 2008 *Solid State Commun.* **147** 436
[17] Cho E J, Oh S J, Imada S, Suga S, Suzuki T and Kasuya T 1995 *Phys. Rev.* B **51** 10146
[18] Liebsch T, Hentges R, Rüdel A, Viefhaus J, Becker U and Schlögl R 1997 *Chem. Phys. Lett.* **279** 197
[19] Wang X X, Li H N, Zhang W H and Xu F Q 2007 *J. Phys.: Condens. Matter* **19** 096001
[20] He S L, Li H N, Wang X X, Li H Y, Xu Y B, Bao S N, Ibrahim K, Qian H J, Su R, Zhong J, Hong C H and Abbas M I 2005 *Phys. Rev.* B **71** 085404
[21] He S, Nakatake M, Arita M, Cui X, Qiao S, Namatame H, Taniguchi M, Li H Y and Li H N 2007 *Appl. Phys. Lett.* **91** 143103
[22] Wang X X, Li H N, Qian H J, Su R, Zhong J, Hong C H and Wang J O 2006 *Acta Phys. Sin.* **55** 4265 (in Chinese)
[23] Yoshikawa H, Kuroshima S, Hirosawa I, Tanigaki K and Mizuki J 1995 *Chem. Phys. Lett.* **239** 103
[24] Wang X X, Li H N, Xu Y B, Wang P, Zhang W H and Xu F Q 2009 *Chin. Phys. Lett.* **26** 017104
[25] Andreoni W, Giannozzi P, Armbruster J F, Knupfer M and Fink J 1996 *Europhys. Lett.* **34** 699
[26] Turek I, Kudrnovský J, Diviš M, Franek P, Bihlmayer G and Blügel S 2003 *Phys. Rev.* B **68** 224431
[27] Kuneš J and Laskowski R 2004 *Phys. Rev.* B **70** 174415
[28] Li H N, He S L, Zhang H J, Lu B, Bao S N, Li H Y, He P M and Xu Y B 2003 *Phys. Rev.* B **68** 165417
[29] Yamamoto K, Horiba K, Taguchi M, Matsunami M, Kamakura N, Chainani A, Takata Y, Mimura K, Shiga M, Wada H, Senba Y, Ohashi H and Shin S 2005 *Phys. Rev.* B **72** R161101
[30] Cho E J and Oh S J 1999 *Phys. Rev.* B **59** R15613